Optical Biosensors for COVID-19 and Other Viruses Diagnosis

Subjects: Engineering, Biomedical | Infectious Diseases | Biophysics

Contributor: Pauline John , Nilesh J. Vasa , Azhar Zam

The sudden outbreak of the COVID-19 pandemic led to a huge concern globally because of the astounding increase in mortality rates worldwide. The medical imaging computed tomography technique, whole-genome sequencing, and electron microscopy are the methods generally used for the screening and identification of the SARS-CoV-2 virus.

COVID-19 virus | optical spectroscopy | optical biosensors | optical diagnosis | optical therapy | artificial intelligence | Internet of Things | machine learning

1. Introduction

In recent times, COVID-19 played havoc, causing escalating mortality rates globally. According to the World Health Organization (WHO), on 21 February 2023, 757,264,511 confirmed cases and 6,850,594 deaths related to COVID-19 were reported globally [1]. The history of viral pandemic diseases, including the Spanish flu, which originated in 1918, severe acute respiratory syndrome (SARS), and the Middle East respiratory syndrome (MERS), which originated a decade ago, and the recent emergence of a novel coronavirus caused by the SARS-CoV-2 virus.

The MERS, SARS, and SARS-CoV-2 viruses are considered the most lethal respiratory diseases transmitted by zoonotic transmission, leading to death in patients with severe comorbid conditions [2][3]. They are highly contagious among humans. Each type of virus is distinctively characterized based on its surface proteins and lipid profiles. Coronavirus belongs to the subfamily Coronaviridae and is an enveloped RNA virus 100–160 nm in diameter, with a spherical structure. This subfamily, based on phylogenetic relationships and genomic structures, is classified into four groups: (i) alpha coronavirus, (ii) beta coronavirus, which infects mammals, (iii) gamma coronavirus, which infects aves, and (iv) delta coronavirus, which infects both aves and mammals [2]. Coronavirus has the single-stranded positive-sense RNA (ssRNA) genetic material and the largest genome of 26.4–31.7 kb, which encodes the structural proteins such as spike glycoprotein (S), membrane glycoprotein (M), nucleocapsid interrupts phosphor protein (N), and envelope (E) protein [2][3][4]. The genome of SARS-CoV-2 shares 82% of its sequence identity with SARS-CoV and MERS-CoV and more than 90% of its sequence identity with that of structural proteins and essential enzymes. Coronavirus uses the spike protein (S) to bind to the receptor of the host cell surface and initiate infection. The mechanism of host entry differs for different coronaviruses [5]. A more detailed discussion on the genomics, proteomics, and mechanism of pathogenesis of SARS-CoV-2 has been reported as a breakthrough therapy [2].

2. Optical Biosensors

2.1. Spectroscopy and Nanomaterials-Based Optical Biosensors

Advancements in science and technology have led to the growth of spectroscopic techniques in clinical and biological studies. A retrospective review of spectroscopic techniques used in the diagnosis of viral infection for a decade (2006–2016) has been reported by one of the research groups and includes nuclear magnetic resonance spectroscopy, near-infrared spectroscopy, Raman spectroscopy, surface-enhanced Raman spectroscopy (SERS), and molecular fluorescence spectroscopy [6]. In addition to spectroscopy-based optical techniques such as Raman spectroscopy and SERS, molecular fluorescence spectroscopy and infrared spectroscopy have also been demonstrated for detecting viruses [7][8][9][10][11][12]. The non-optical spectroscopic nuclear magnetic-resonance-based method has also been discussed for the detection of viruses [13][14]. Processing and analyzing large amounts of spectroscopic data is challenging, requiring computational analysis, which includes pre-processing, and multivariate analysis such as principle component analysis (PCA), cluster analysis (CA), genetic algorithm (GA), successive projections algorithm, the partial least square (PLS) method, and the linear regression analysis (LRA) method, mostly combined with PCA and PLS [6].

2.1.1. Raman Spectroscopy

Raman spectroscopy works on the phenomenon of inelastic scattering, wherein a monochromatic light source is employed in detecting the presence of polar and non-polar chemical bonds present in the sample, along with their cellular changes. In addition to their non-destructive, reagent-less, non-contact capability of detecting the unique spectral fingerprints of molecules, the insignificant Raman scattering of water is the main advantage of utilizing this approach in biological studies compared to other techniques like NIR spectroscopy and Fourier transform IR spectroscopy.

Raman spectroscopy and surface-enhanced Raman spectroscopy techniques have been widely considered for the detection of several types of viruses such as herpes simplex virus type 1 (HSV-1), hepatitis C virus, ALVAC virus, tobacco mosaic virus, and several other emerging new influenza viruses [7][8][9][10][11][12][15]. The detection of structural changes of nucleic acids, proteins, and lipids of HSV-1 was observed with a sensitivity close to 100% in the Raman spectrum range of 1195–1726 cm^{-1}, by which they could differentiate the controlled group from the infected cells [16].

Another group has demonstrated Raman spectroscopy-based label-free early detection of adenovirus-infected human embryonic kidney epithelial (HEK293) cells at 12, 24, and 48 h after instigating the infection [17]. Principle component analysis has been incorporated for classifying infected cells from control cells. A continuous wave Ti:sapphire laser source with an excitation wavelength of 785 nm has been used to detect bands at 1003 cm^{-1} and 1440 cm^{-1}, which are attributed to phenylalanine and the CH deformation mode, respectively.

2.1.2. Near-Infrared and Fourier Transform Infrared Spectroscopy

Non-invasive and nondestructive near-infrared (NIR) spectroscopy has been widely used in several clinical applications, mainly because of the fast detection, without requiring reagents or sample preparation. The “optical window” region of 650–1100 nm in the near-infrared (NIR) wavelength region of 700–2500 nm is the suitable region for the measurement of biomolecules such as proteins, lipids, and carbohydrates [12]. Stretching, bending, rocking, and scissoring are the various vibratory motions of different chemical bonds that result in absorption in the infrared region. The stretching and bending vibrations of functional groups of C-H, O-H, and N-H bonds result in absorption in the NIR region. Detection of human immunodeficiency virus type-1 (HIV-1) subtypes using NIR spectroscopy has been demonstrated [10]. Absorption wavelengths at 682 nm, 948 nm, 1028 nm, and 1058 nm were used to discriminate different subtypes of HIV-1. Absorption around 950 nm has been considered to be the prominent peak for HIV-1, which occurs as a result of the absorption combination tone of ($2\nu_1 + \nu_2$), i.e., symmetric stretching vibration of O-H (ν_1) and asymmetric stretching vibration of O-H (ν_2) [12]. On the other hand, in the mid-IR region of 400–4000 cm^{-1}, a range of 900–1800 cm^{-1} is attributed to the “bio fingerprint” region for sensing biological samples. The spectral bands at ~1750 cm^{-1}, 1155 cm^{-1}, 1650 cm^{-1}, 1550 cm^{-1}, 1260 cm^{-1}, 1225 cm^{-1}, and 1080 cm^{-1} have been observed to be attributed to lipids, carbohydrates, proteins amide I, amide II, amide III, DNA, and RNA, respectively.

Comparison of the NIR-based Raman spectroscopy technique with standard serological ELISA test and the molecular PCR technique has been demonstrated for classifying healthy human blood serum and viral hepatitis-C-infected human blood serum [18]. This method utilizes a semiconductor laser source with an excitation wavelength at 830 nm and incorporates multivariate analysis methods such as principal component analysis (PCA) for spectral feature extraction and the Mahalanobis distance method for blood sample classification. The Raman bands at 1170 cm^{-1}, 1257 cm^{-1}, and 1344 cm^{-1} are attributed to the CO-O-C asymmetric stretching in lipids and CH_2 wagging band in biomarkers—phospholipids get activated by the hepatocytes process in hepatitis C blood serum. These significant bands at 1002 cm^{-1}, 1170 cm^{-1}, 1257 cm^{-1}, and 1344 cm^{-1} are the regions where the most prominent differences between healthy and hepatitis C spectra were reported [18]. The NIR Raman-spectroscopy-technique-based detection, compared to conventional chemiluminescence analysis, was reported to classify hepatitis-C-infected human blood serum from healthy human blood serum with a sensitivity of 92%.

2.1.3. Gold-Nanoparticle-Based Surface Plasmon Resonance

The optical, mechanical, electronic, and magnetic properties of nanomaterials, such as metal nanoparticles, carbon nanotubes, silica nanoparticles, fluorescent quantum dots, plasmonic gold nanoparticles, silver nanocrystals, and polymeric nanoparticles, have a great impact on clinical research and have envisioned applications in biosensing, biomedical imaging, and clinical diagnosis [19]. Noble nanoparticles, specifically metal and gold nanoparticles (AuNPs) ranging from 1 to 800 nm in size, used as nanoprobes for the diagnosis of various types of viruses have outpaced other materials because of their outstanding stability, biocompatibility, strong fluorescence, excellent photostability, and long emissive lifetimes and their intense color providing ease in visualizing as labeling agents. They have been inevitable in detecting the targets of pathogenic viruses, such as the antigens, capsid proteins, and specific gene segments in their genome. They are also observed to form stable bioconjugates with biomolecules to aid in virus detection with high sensitivity and specificity [20]. They are synthesized using several

methods such as ultraviolet irradiation, laser ablation, lithography, and photochemical reduction of Au to form different morphological shapes and hollow structures. Resonance light scattering detection using localized surface plasmon resonance (LSPR) and Raman spectroscopy, color amplification detection using the colorimetric technique, and fluorescence quenching, and fluorescence enhancement are the optical signal transduction functions of AuNPs in the detection of viruses [21][22][23][24][25][26][27][28]. LSPR-based detection of influenza virus particles by conjugating a peptide linker with a QD and AuNP, demonstrating alteration in the intensity of absorption in the presence of influenza virus particles, has been reported [29].

2.1.4. Gold-Nanoparticle-Based Surface-Enhanced Raman Spectroscopy

The surface-enhanced Raman spectroscopy (SERS) approach is a substitute to overcome the limitation of detecting weak signals generated in conventional Raman spectroscopy and is said to have sensitivity and specificity from 10^4 to 10^9 higher than conventional Raman spectroscopy. It is a widely used application in detecting viruses, cancerous cells, and biological imaging. An indirect method of detecting specific viruses by tagging the antibodies induced by them with nanoparticles of 150 nm has been demonstrated by generating surface-enhanced Raman spectroscopy signals [30]. The SERS active Ag-Au nano-wave chip, functionalized by a DNA probe, has also been employed in the detection of specific oligonucleotide sequences of the dengue virus with fewer false-positive errors [31].

2.1.5. Magnetic-Nanoparticle-Based Fluorescence Biosensors

Quantum dots used in fluorescence biosensors are advantageous in terms of high quantum yield, tunability of emission wavelength, photostability, and Stokes shift compared to small-molecule organic dyes. However, their high cytotoxicity in oxidative environments and the possible damage of DNA is a major concern for long-term in vivo studies [32]. As an alternative, conjugated polymer nanoparticles and carbon dots are developed as biocompatible light-emitting nanomaterials. Optical detection of coronavirus by synthesizing chiral zirconium quantum dots (Zr QDs) of 2–3 nm size was reported to exhibit fluorescence at 412 nm and absorbance at 378 nm [33]. A change in the fluorescence intensity with varying concentrations of virus solution has been reported. Biosensing of coronavirus and infectious bronchitis virus (IBV) with a detection limit of 79.15 EID/50 µL has been reported by the fluorescence properties of nanohybrid conjugate with quantum dots and magneto-plasmonic nanoparticles, through separation by an external magnetic field. It is also reported that this technique has achieved 10 times higher sensitivity compared to the conventional ELISA technique [33]. The promising features of Zr QDs, such as optical chirality, nontoxicity, biocompatibility, strong fluorescence emission tunable across the visible and infrared ranges, broad excitation wavelength, optical and thermal stability, mechanical strength, and better quantum yield, would significantly benefit their use in the field of biosensing [33]. The tremendous potential of these nanoparticle-based biosensors could replace or enhance the performance of existing virus detection methods. Optical fluorescence-based biosensors are widely used in the detection of viruses because of their accuracy and sensitivity in detection. A three-dimensional copper-based metal–organic framework has been utilized based on the fluorescence technique to detect dengue and Zika viruses with detection limits of 184 and 121 pM, respectively [34].

2.2. Interferometry-Based Optical Biosensors

The refractive index is one of the fundamental optical parameters used for the label-free sorting of materials, including viruses. It is challenging to detect the refractive index of biological material with high precision because of its heterogeneous nature. Application of optical cavity resonance, surface plasmon resonance, and optical interferometry approaches aid in indirect measurement of the refractive index by the measurement of spectral shift, size of the virions, and density of the virions bound on an antibody-sensing surface [35]. This phenomenon of refractive-index-based spectral shift, which is attributed to the change in the concentration of the analyte such as glucose, has also been reported for non-invasive and selective detection of the analyte using a frequency domain dual-wavelength low-coherence interferometry system in the NIR wavelength region [36][37].

2.2.1. Photonic Crystal Biosensors

Optical label-free photonic crystal biosensors have also been designed and developed for rapid detection of viruses such as the dengue virus, with a high sensitivity, based on the measurement of refractive index change on a photonic crystal [38]. A unique geometry of a photonic crystal biosensor waveguide with five resonators has been designed to distinguish multiple analytes simultaneously. Replacement of bulky spectrometers with vertical-cavity surface-emitting laser systems have also been considered and utilized for detecting human anti-dengue IgG antibodies [39]. However, false-positive errors and low specificity were the drawbacks of this technique.

2.2.2. Back Focal Plane Interferometry

Optical trapping of a single virion with optical tweezers is considered for the measurement of the refractive index and size of the virions, based on their dependence on the stiffness of the optical trap. A novel method based on an optical tweezer using back focal plane interferometry, for measurement of the refractive index of a single human immunodeficiency virus type-1 (HIV-1) with high precision in aqueous media, has been demonstrated using a tapered amplifier diode laser of wavelength 830 nm and a laser power of 130.8 mW, resulting in a refractive index of 1.42, with less than a 2% coefficient of variation [40].

2.2.3. Mach–Zehnder Interferometry

Figure 1 describes the mechanism of the evanescent wave, where a variation in the refractive index is detected when there is a biomolecular interaction at the surface of the waveguide. A simple Mach–Zehnder interferometer configuration incorporated with a closed-loop flow system based on the principle of the evanescent wave, which enables measurement of the interference of two light beams (laser diode light source of 670 nm wavelength and 5 mW power), one that passes through a waveguide that acts as a biosensor with antibody coupled on to its surface and the other one that is the reference beam that is not functionalized with the bioreceptor, thereby to detect the avian influenza virus, has been designed. As the target binds to the bioreceptor immobilized on the surface of the waveguide, the water molecules get displaced and its structure gets altered, resulting in the velocity change of the light beam that propagates. The phase of the interference pattern is measured using the Fourier transform algorithm, with a detection sensitivity of 0.01 rad and a change in the refractive index of less than 10^{-6}. A detection limit as low as 0.0005 HA (hemagglutination—antigen-specific) units/mL of virus concentrations has been reported [41].

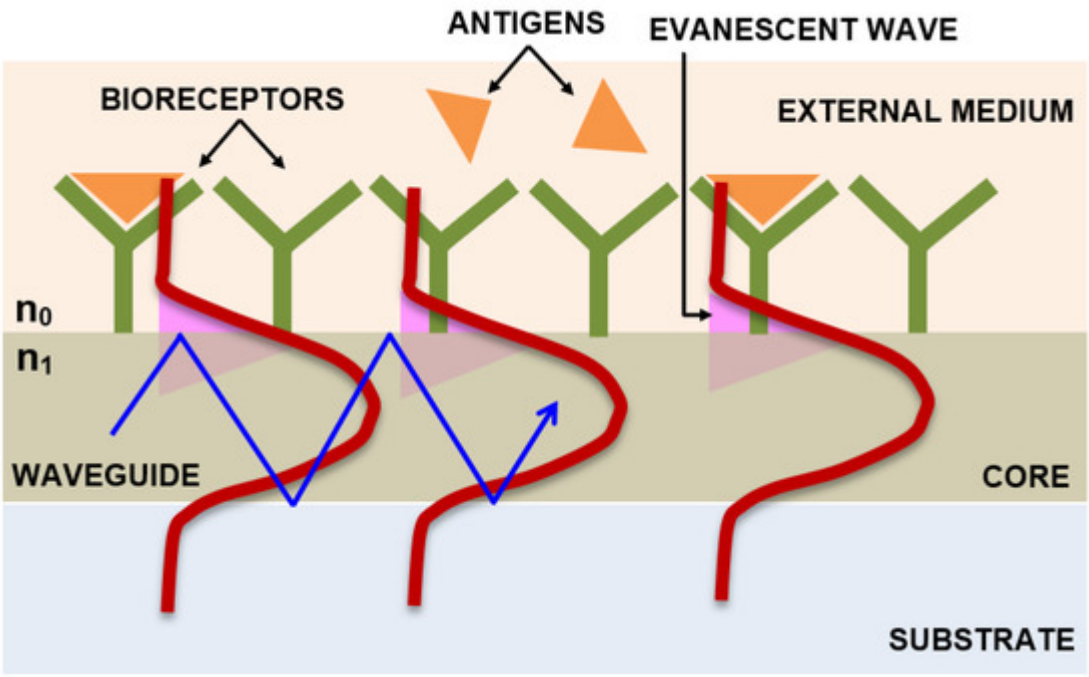

Figure 1. Schematic representation showing the interaction of biomolecules with the waveguide surface within the evanescent field.

2.2.4. Integrated Optical Young's Interferometry

A four-channel, integrated optical Young interferometry technique, using a monochromatic argon laser light source and a CCD camera, has been reported for selective and sensitive detection of herpes simplex virus type 1 (HSV-1) at very low concentrations of 850 particles/mL [42]. Three appropriate antibody-coated waveguide channels have been used to measure different analytes, and the fourth channel has been used as a reference channel. A corresponding phase change resulting from the interference pattern measured from the evanescent wave that has been used to probe the analyte binding to the antibody surface has been measured.

For the HSV-1 particle size of 150–200 nm and refractive index of ~1.4, a phase change of ~1.1×10^{-4} fringes for a single virus particle has been reported. This system was further developed into a handheld device by integrating a glass microfluidic system with a four-channel Young interferometer optical chip [43]. The goal of this approach was to achieve a shorter response time of 5 s using a disposable chip, compared to the 100 s that was previously achieved using a bulky cuvette, as well as to aid in simultaneous and multiplexed detection of numerous pathogenic species.

2.2.5. Interferometry Reflectance Imaging Sensor

Another label-free high-throughput technique demonstrated for single-virus and viral antigen detection is the interferometric reflectance imaging sensor (IRIS) [44]. This system is based on an imaging approach that includes measurement of phase changes in the interference response resulting from reflections from a layered substrate, as

shown in **Figure 2**. This approach has been reported to have detected vesicular stomatitis virus, with a detection limit of 5 × 10^3 PFU/mL.

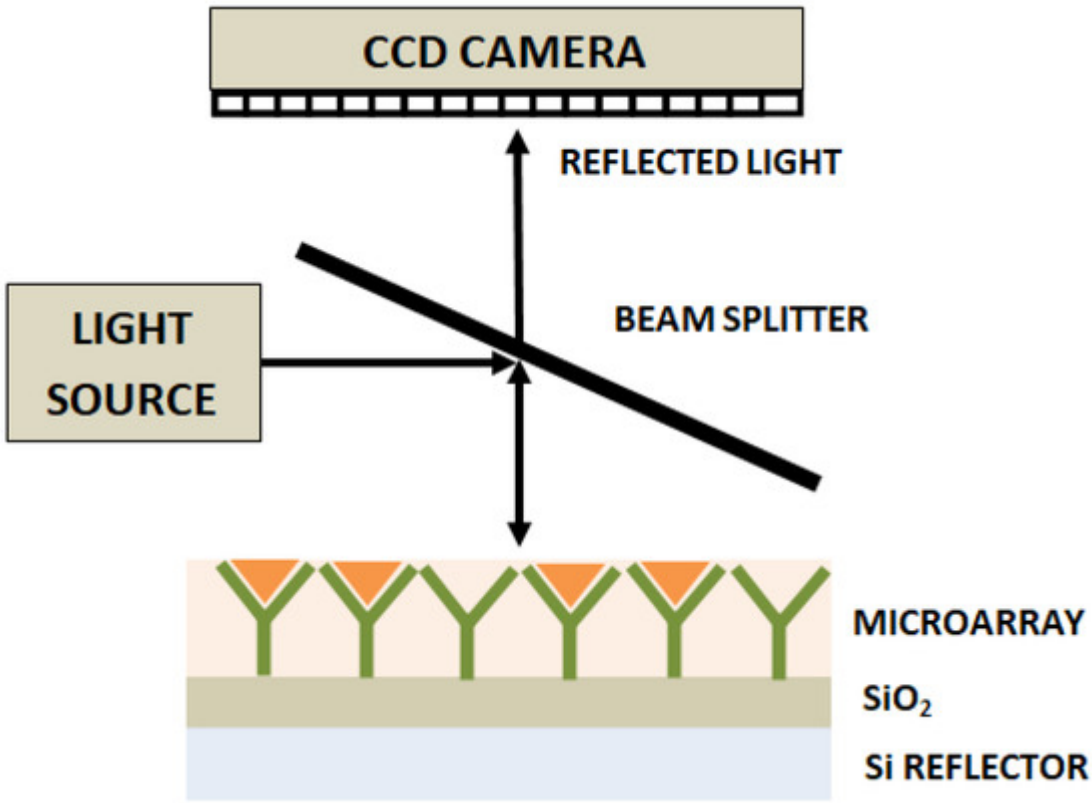

Figure 2. Schematic representation of interferometric reflectance imaging sensor (IRIS).

2.2.6. Hartman Interferometer

In contrast to the Mach–Zehnder and Young's interferometry techniques, the Hartman interferometer utilizes a planar waveguide and allows interaction of a broad beam of linearly polarized light with the multiple sensing regions on the chip or a waveguide film, fabricated using photolithographic techniques. Individual interferometers have been created on a single chip by immobilizing both specific and nonspecific probes on different regions, thereby allowing multiplexed detection. A photodiode array has been utilized to measure the exiting light from the waveguide. This sensor has been reported to perform the detection of the influenza-A virus with a sensitivity of 2 × 10^6 PFU/mL [45].

2.2.7. Liquid Core Optical Ring Resonator

A liquid core optical ring resonator (LCORR) has been designed using a cylindrical capillary tube that supports the whispering gallery mode (WGM) [46]. The setup includes an on-chip waveguide-coupled LCORR where the light is coupled through this capillary tube that acts as an optical ring resonator. The analytes are detected as a result of the interaction of the evanescent field from the WGM with the analytes bound to the inner surface of the capillary [47]. Utilizing this technique, the detection of filamentous viruses of 10 nm diameter, with a spectral shift and detection limit of 2 pm and 2.3 × 10^3 PFU/mL, respectively, has been reported [48].

2.3. Lab-on-a-Chip-Based Optical Biosensors

Several reviews highlight the need for developing a lab-on-a-chip (LOC)-based technique to replace the time-consuming cell culturing method and expensive electron-microscopy-based identification of viral particles, which necessitates technical skills and expertise. Although flow cytometry, enzyme-linked immunosorbent assay (ELISA) and polymerase chain reaction (PCR) provide high sensitivity and specificity in detecting viruses, they are expensive, time consuming, and labor intensive and require well-trained operators. Although it is possible to couple spectrophotometers, lasers, and microscopes to LOCs, the miniaturization and portability of the detection system is challenging [49]. The introduction of integrated microfluidic LOC devices has an enormous impact on biosensing with a miniaturized platform, initiating cost-effective and rapid diagnosis of viral bodies. Fabrication techniques such as laser ablation, micro-electromechanical system (MEMS) technique, and soft lithography have been used for developing LOC structures [50]. Biodegradable, disposable, and portable paper-based LOC structures such as lateral flow strips (LFS) have also been widely used in diagnostics [50].

An integrated hand-held fluorescent probe system utilizing an LED source to excite the fluorophore at 490 nm has been used to detect the RNA of H5N1 avian influenza virus and Ebolavirus [51]. A similar portable microfluidic PCR platform based on real-time fluorescence detection of hepatitis B virus has been demonstrated with an LED source for exciting the fluorescent dye at a wavelength of 475 ± 10 nm, incorporated with an emission filter at 525 ± 25 nm and a proportional integral derivative algorithm for temperature control. A detection limit of 100 copies/μL DNA was reported to be detected within an hour, with an efficiency of 98.76% [52]. Microfluidic paper-based analytical devices have also been reported to detect the viral protein of 10 ng mL^{-1} in blood and plasma in ≈7 min [53].

2.4. Smartphone-Based Portable Optical Biosensors

Compact and portable handheld, easily operable point-of-care devices for real-time virus detection are essential in remote locations that lack sophisticated laboratory facilities. Disposable chip sensors based on electrochemical, optical, magnetic, mechanical, thermometric, and microgravimetric quartz crystal microbalance (QCM) methods used for medical diagnostics, food, and environmental analysis have been reported [54]. Among these, optical-technique-based disposable sensors integrated with smartphones is advantageous because of their reliability, sensitivity, non-destructivity, fast sensing, and multiplexing capability [55]. The smart detecting capability of photo cameras, the smart recording capability of image sensors, the smart readout capability of smartphones, and built-in LED that act as smart light sources have led to growing interest among researchers in combining microfluidic chips and micro-biosensors to smartphones for detecting biological constituents such as enzymes, nucleic acids, cells, antigens–antibodies, whole viruses, and microorganisms [56].

A hand-held, fluorescence-based iPhone 5S smartphone used for the in situ detection of proteins with a detection limit of 10 pg/mL has been reported [56]. In this technique, a fluorescence nanoparticle immunoagglutination assay incorporated into an organ-on-chip (OOC)-based smartphone biosensor has been fabricated to enable simulation of the response of human kidneys to nephrotic drugs. Elsewhere, the Y-channel OOC device has been fabricated, wherein the smartphone-based fluorescent microscope consisting of three white LEDs, an objective lens, 480 ± 10

nm bandpass filter for the light source, 500 nm long pass filter for the smartphone camera, 3 V button batteries to power the LED sources, a secondary objective lens, and the smartphone camera, which acts as an image-capturing device are incorporated to measure the fluorescence scatter intensities from the Y-channel OOC.

Internet of Things (IoT)-assisted smartphone-based optical biosensors, working on artificial intelligence (AI) platforms, could aid in the sensing or imaging, acquisition, and collection of big data from the sensor, thereby providing support in the prediction of a pandemic outbreak of COVID-19 to track its spread and provide diagnosis and vaccine discovery. With the advances in wearable techniques, wearable smart watches, or wearable patch-integrated smartphones for signal transmission could be invented for rapid and effective screening and tracking of coronavirus-infected subjects, thereby providing efficient control over the spread of the disease [57].

2.5. Artificial-Intelligence-Based Smart Optical Biosensors

In the case of imaging techniques, automated detection and classification of large data images of subjects infected with coronavirus are crucial. The emergence of IoT and AI find their applications in tackling big data outcomes from various fields, among which the handling of big data related to health care is greatly beneficial [58][59][60]. Using deep learning (DL) approaches, screening models to differentiate pulmonary CT images of COVID-19 cases from healthy and influenza-A viral pneumonia have been demonstrated with an accuracy of 86.7% [61]. A flow chart with five layers of the AI-based approach in diagnosis and tracing of COVID-19, consisting of (i) input database layer, (ii) selection layer, (iii) imaging layer which includes magnetic resonance imaging (MRI), X-ray, computed tomography (CT), positron emission tomography (PET) and optical microscopy imaging, (iv) optimization layer, and (v) output diagnosis layer, has been described [62]. The traditional optical microscope approach is the main tool used in the investigation of pathological conditions.

A detailed explanation of the various AI-based DL approaches, such as extreme learning machine (ELM), recurrent neural network (RNN), generative adversarial networks (GANs), and long/short-term memory (LSTM), have also been provided for combating COVID-19 [62]. Another group has presented a novel automated screening technique to detect COVID-19 by converting histograms of bio-optical attributes obtained from digital holographic-microscopy-reconstructed red blood cells to feature vectors using the bag-of-features (BoF) method, followed by classification using the linear support vector machine (SVM), with an accuracy, sensitivity, and specificity of 91.67%, 90%, and 92.86%, respectively [63]. The risk of deterioration of patients infected with COVID-19 was predicted automatically by another research group from chest X-rays using a deep convolution neural network along with other clinical predictors, which include vital signs and lab tests. This helps in decision making and prioritizing patients who need immediate emergency treatment [64]. This multi-modal system based on the globally aware multiple instance classifier and gradient boosting model has been successfully used during the first wave of the pandemic at New York University Langone Health and achieved the area under the curve of 0.786. Elsewhere, an IoT-based unmanned aerial vehicle (UAV) incorporated with GPS and thermal cameras to measure human body temperature and a deep learning model to detect people with and without face masks has been proposed to control the spread of the virus [65].

3. Conclusions

In addition to the diagnostic applications of nanoparticles in the optical detection of viruses, they also have a great potential in therapeutic applications against viruses because of their high surface-to-volume ratio, which allows them to interfere with and block viral entry into the cell [66][67]. It requires engineered nanomaterials to inactivate the viruses or inhibit viral binding to the surface receptor of the host cell. Carbon quantum dots (CQDs) of average diameter below 10 nm have been employed to study the antiviral properties and inhibition of viral activities related to human coronavirus HCoV-229E [68]. However, further in vivo experimental studies to validate its function on other coronaviruses are essential. A nanomaterial-based photodynamic therapy (PDT) has also been suggested to be an effective therapeutic method for viruses [69][70]. PDT is an approved technique used in cancer treatment [71]. It requires a photosensitizer, which when excited by a visible light reacts with dioxygen, forming reactive oxygen species (ROS) that can in turn react with biological molecules such as proteins, lipids, and nucleic acids, causing oxidation and finally leading to irreversible damage to the cells and tissues. Delivery of photosensitizers such as indocyanine green into the cells of the lungs and intra-tracheal and laser therapy or activation by an 810 nm laser source has been suggested to be a potential method against coronavirus [72].

References

1. WHO Coronavirus (COVID-19) Dashboard. Available online: https://covid19.who.int/ (accessed on 16 April 2023).
2. Naqvi, A.A.T.; Fatima, K.; Mohammad, T.; Fatima, U.; Singh, I.K.; Singh, A.; Atif, S.M.; Hariprasad, G.; Hasan, G.M.; Hassan, M.I. Insights into SARS-CoV-2 genome, structure, evolution, pathogenesis and therapies: Structural genomics approach. Biochim. Biophys. Acta BBA-Mol. Basis Dis. 2002, 1866, 165878.
3. Cui, J.; Li, F.; Shi, Z.L. Origin and evolution of pathogenic coronaviruses. Nat. Rev. Microbiol. 2019, 17, 181–192.
4. Pellett, P.E.; Mitra, S.; Holland, T.C. Basics of virology. Handb. Clin. Neurol. 2014, 123, 45–66.
5. Lau, Y.L.; Peiris, J.M. Pathogenesis of severe acute respiratory syndrome. Curr. Opin. Immunol. 2005, 17, 404–410.
6. Santos, M.C.; Morais, C.L.; Nascimento, Y.M.; Araujo, J.M.; Lima, K.M. Spectroscopy with computational analysis in virological studies: A decade (2006–2016). TrAC Trends Anal. Chem. 2017, 97, 244–256.
7. Chaudhary, I.; Jackson, N.; Denning, D.; O'Neill, L.; Byrne, H.J. Contributions of vibrational spectroscopy to virology: A review. Clin. Spectrosc. 2022, 4, 100022.

8. Moor, K.; Ohtani, K.; Myrzakozha, D.; Zhanserkenova, O.; Andriana, B.B.; Sato, H. Noninvasive and label-free determination of virus infected cells by Raman spectroscopy. J. Biomed. Opt. 2014, 19, 067003.
9. Santos, M.C.; Monteiro, J.D.; Araújo, J.M.; Lima, K.M. Molecular fluorescence spectroscopy with multi-way analysis techniques detects spectral variations distinguishing uninfected serum versus dengue or chikungunya viral infected samples. Sci. Rep. 2020, 10, 13758.
10. Rodríguez-Casado, A.; Bartolomé, J.; Carreño, V.; Molina, M.; Carmona, P. Structural characterization of the 5′ untranslated RNA of hepatitis C virus by vibrational spectroscopy. Biophys. Chem. 2006, 124, 73–79.
11. Kim, H.; Hwang, J.; Kim, J.H.; Lee, S.; Kang, M. Sensitive detection of multiple fluoresence probes based on surface-enhanced Raman scattering (sers) for mers-cov. In Proceedings of the 2019 IEEE 14th International Conference on Nano/Micro Engineered and 776 Molecular Systems (NEMS), Bangkok, Thailand, 11–14 April 2019; pp. 498–501.
12. Sakudo, A.; Suganuma, Y.; Sakima, R.; Ikuta, K. Diagnosis of HIV-1 infection by near-infrared spectroscopy: Analysis using molecular clones of various HIV-1 subtypes. Clin. Chim. Acta 2012, 413, 467–472.
13. Amathieu, R.; Triba, M.N.; Goossens, C.; Bouchemal, N.; Nahon, P.; Savarin, P.; Le Moyec, L. Nuclear magnetic resonance based metabolomics and liver diseases: Recent advances and future clinical applications. World J. Gastroenterol. 2016, 22, 417.
14. Slupsky, C.M. Nuclear magnetic resonance-based analysis of urine for the rapid etiological diagnosis of pneumonia. Expert Opin. Med. Diagn. 2011, 5, 63–73.
15. Lambert, P.J.; Whitman, A.G.; Dyson, O.F.; Akula, S.M. Raman spectroscopy: The gateway into tomorrow’s virology. Virol. J. 2006, 3, 51.
16. Salman, A.; Shufan, E.; Zeiri, L.; Huleihel, M. Characterization and detection of Vero cells infected with Herpes Simplex Virus type 1 using Raman spectroscopy and advanced statistical methods. Methods 2014, 68, 364–370.
17. Kelly, J.G.; Trevisan, J.; Scott, A.D.; Carmichael, P.L.; Pollock, H.M.; Martin-Hirsch, P.L.; Martin, F.L. Biospectroscopy to metabolically profile biomolecular structure: A multistage approach linking computational analysis with biomarkers. J. Proteome Res. 2011, 10, 1437–1448.
18. Saade, J.; Pacheco, M.T.T.; Rodrigues, M.R.; Silveira, L., Jr. Identification of hepatitis C in human blood serum by near-infrared Raman spectroscopy. Spectroscopy 2008, 22, 387–395.
19. Howes, P.D.; Chandrawati, R.; Stevens, M.M. Colloidal nanoparticles as advanced biological sensors. Science 2014, 346, 1247390.

20. Baptista, P.; Pereira, E.; Eaton, P.; Doria, G.; Miranda, A.; Gomes, I.; Quaresma, P.; Franco, R. Gold nanoparticles for the development of clinical diagnosis methods. Anal. Bioanal. Chem. 2008, 391, 943–950.
21. Neng, J.; Harpster, M.H.; Wilson, W.C.; Johnson, P.A. Surface-enhanced Raman scattering (SERS) detection of multiple viral antigens using magnetic capture of SERS-active nanoparticles. Biosens. Bioelectron. 2013, 41, 316–321.
22. Cao, Y.C.; Jin, R.; Mirkin, C.A. Nanoparticles with Raman spectroscopic fingerprints for DNA and RNA detection. Science 2002, 297, 1536–1540.
23. Griffin, J.; Singh, A.K.; Senapati, D.; Rhodes, P.; Mitchell, K.; Robinson, B.; Yu, E.; Ray, P.C. Size- and distance-dependent nanoparticle surface-energy transfer (NSET) method for selective sensing of hepatitis C virus RNA. Chem. A Eur. J. 2009, 15, 342–351.
24. Lu, X.; Dong, X.; Zhang, K.; Han, X.; Fang, X.; Zhang, Y. A gold nanorods-based fluorescent biosensor for the detection of hepatitis B virus DNA based on fluorescence resonance energy transfer. Analyst 2013, 138, 642–650.
25. Nasrin, F.; Chowdhury, A.D.; Takemura, K.; Lee, J.; Adegoke, O.; Deo, V.K.; Abe, F.; Suzuki, T.; Park, E.Y. Single-step detection of norovirus tuning localized surface plasmon resonance-induced optical signal between gold nanoparticles and quantum dots. Biosens. Bioelectron. 2018, 122, 16–24.
26. Chang, Y.F.; Wang, S.F.; Huang, J.C.; Su, L.C.; Yao, L.; Li, Y.C.; Wu, S.C.; Chen, Y.M.A.; Hsieh, J.P.; Chou, C. Detection of swine-origin influenza A (H1N1) viruses using a localized surface plasmon coupled fluorescence fiber-optic biosensor. Biosens. Bioelectron. 2010, 26, 1068–1073.
27. Ganbold, E.O.; Kang, T.; Lee, K.; Lee, S.Y.; Joo, S.W. Aggregation effects of gold nanoparticles for single-base mismatch detection in influenza A (H1N1) DNA sequences using fluorescence and Raman measurements. Colloids Surf. B Biointerfaces 2012, 93, 148–153.
28. Draz, M.S.; Fang, B.A.; Li, L.; Chen, Z.; Wang, Y.; Xu, Y.; Yang, J.; Killeen, K.; Chen, F.F. Hybrid nanocluster plasmonic resonator for immunological detection of hepatitis B virus. ACS Nano 2012, 6, 7634–7643.
29. Nasrin, F.; Chowdhury, A.D.; Takemura, K.; Kozaki, I.; Honda, H.; Adegoke, O.; Park, E.Y. Fluorometric virus detection platform using quantum dots-gold nanocomposites optimizing the linker length variation. Anal. Chim. Acta 2020, 1109, 148–157.
30. Li, Y.; Lu, C.; Zhou, S.; Fauconnier, M.L.; Gao, F.; Fan, B.; Lin, J.; Wang, F.; Zheng, J. Sensitive and simultaneous detection of different pathogens by surface-enhanced Raman scattering based on aptamer and Raman reporter co-mediated gold tags. Sens. Actuators B Chem. 2020, 317, 128182.

31. Ngo, H.T.; Wang, H.-N.; Fales, A.M.; Nicholson, B.P.; Woods, C.W.; VoDinh, T. DNA bioassay-on-chip using SERS detection for dengue diagnosis. Analyst 2014, 139, 5655–5659.
32. Maddali, H.; Miles, C.E.; Kohn, J.; O'Carroll, D.M. Optical biosensors for virus detection: Prospects for SARS-CoV-2/COVID-19. ChemBioChem 2021, 22, 1176–1189.
33. Ahmed, S.R.; Kang, S.W.; Oh, S.; Lee, J.; Neethirajan, S. Chiral zirconium quantum dots: A new class of nanocrystals for optical detection of coronavirus. Heliyon 2018, 4, e00766.
34. Xie, B.P.; Qiu, G.H.; Hu, P.P.; Liang, Z.; Liang, Y.M.; Sun, B.; Bai, L.P.; Jiang, Z.H.; Chen, J.X. Simultaneous detection of Dengue and Zika virus RNA sequences with a three-dimensional Cu-based zwitterionic metal–organic framework, comparison of single and synchronous fluorescence analysis. Sens. Actuators B Chem. 2018, 254, 1133–1140.
35. Fan, X.; White, I.M.; Shopova, S.I.; Zhu, H.; Suter, J.D.; Sun, Y. Sensitive optical biosensors for unlabeled targets: A review. Anal. Chim. Acta 2008, 620, 8–26.
36. John, P.; Vasa, N.J.; Unni, S.N.; Rao, S.R. Glucose sensing in oral mucosa simulating phantom using differential absorption based frequency domain low-coherence interferometry. Appl. Opt. 2017, 56, 8257–8265.
37. John, P.; Vasa, N.J.; Sujatha, N. Glucose sensing in the anterior chamber of the human eye model using supercontinuum source based dual wavelength low coherence interferometry. Sens. Bio-Sens. Res. 2019, 23, 100277.
38. Goddard, J.M.; Mandal, S.; Nugen, S.R.; Baeumner, A.J.; Erickson, D. Biopatterning for label-free detection. Colloids Surf. B Biointerfaces 2010, 76, 375–380.
39. Huang, M.C.; Mateus, C.F.; Foley, J.E.; Beatty, R.; Cunningham, B.T.; Chang-Hasnain, C.J. VCSEL optoelectronic biosensor for detection of infectious diseases. IEEE Photonics Technol. Lett. 2008, 20, 443–445.
40. Pang, Y.; Song, H.; Cheng, W. Using optical trap to measure the refractive index of a single animal virus in culture fluid with high precision. Biomed. Opt. Express 2016, 7, 1672–1689.
41. Xu, J.; Suarez, D.; Gottfried, D.S. Detection of avian influenza virus using an interferometric biosensor. Anal. Bioanal. Chem. 2007, 389, 1193–1199.
42. Ymeti, A.; Greve, J.; Lambeck, P.V.; Wink, T.; van Hövell, S.W.; Beumer, T.A.; Wijn, R.R.; Heideman, R.G.; Subramaniam, V.; Kanger, J.S. Fast, ultrasensitive virus detection using a young interferometer sensor. Nano Lett. 2007, 7, 394–397.
43. Ymeti, A.; Subramaniam, V.; Beumer, T.A.; Kanger, J.S. An ultrasensitive young interferometer handheld sensor for rapid virus detection. Expert Rev. Med. Devices 2007, 4, 447–454.
44. Avci, O.; Lortlar, Ü.N.; Yalçın Özkumur, A.; Ünlü, M.S. Interferometric reflectance imaging sensor (IRIS)—A platform technology for multiplexed diagnostics and digital detection. Sensors 2015, 15,

17649–17665.

45. Schneider, B.H.; Edwards, J.G.; Hartman, N.F. Hartman interferometer: Versatile integrated optic sensor for label-free, real-time quantification of nucleic acids, proteins, and pathogens. Clin. Chem. 1997, 43, 1757–1763.
46. Fan, X.; White, I.M.; Zhu, H.; Suter, J.D.; Oveys, H. Overview of novel integrated optical ring resonator bio/chemical sensors. In Laser Resonators and Beam Control IX; SPIE: Bellingham, Washington USA, 2007; Volume 6452, pp. 166–185.
47. White, I.M.; Oveys, H.; Fan, X.; Smith, T.L.; Zhang, J. Integrated multiplexed biosensors based on liquid core optical ring resonators and antiresonant reflecting optical waveguides. Appl. Phys. Lett. 2006, 89, 191106.
48. Zhu, H.; White, I.M.; Suter, J.D.; Zourob, M.; Fan, X. Opto-fluidic micro-ring resonator for sensitive label-free viral detection. Analyst 2008, 133, 356–360.
49. Pires, N.M.M.; Dong, T.; Hanke, U.; Hoivik, N. Recent developments in optical detection technologies in lab-on-a-chip devices for biosensing applications. Sensors 2014, 14, 15458–15479.
50. Zhu, H.; Fohlerová, Z.; Pekárek, J.; Basova, E.; Neužil, P. Recent advances in lab-on-a-chip technologies for viral diagnosis. Biosens. Bioelectron. 2020, 153, 112041.
51. Ahrberg, C.D.; Manz, A.; Neuzil, P. Palm-sized device for point-of-care Ebola detection. Anal. Chem. 2016, 88, 4803–4807.
52. Li, Z.; Zhao, J.; Wu, X.; Zhu, C.; Liu, Y.; Wang, A.; Deng, G.; Zhu, L. A rapid microfluidic platform with real-time fluorescence detection system for molecular diagnosis. Biotechnol. Biotechnol. Equip. 2019, 33, 223–230.
53. Bedin, F.; Boulet, L.; Voilin, E.; Theillet, G.; Rubens, A.; Rozand, C. Paper-based point-of-care testing for cost-effective diagnosis of acute flavivirus infections. J. Med. Virol. 2017, 89, 1520–1527.
54. Dincer, C.; Bruch, R.; Costa-Rama, E.; Fernández-Abedul, M.T.; Merkoçi, A.; Manz, A.; Urban, G.A.; Güder, F. Disposable sensors in diagnostics, food, and environmental monitoring. Adv. Mater. 2019, 31, 1806739.
55. Quesada-González, D.; Merkoçi, A. Nanomaterial-based devices for point-of-care diagnostic applications. Chem. Soc. Rev. 2018, 47, 4697–4709.
56. Cho, S.; Islas-Robles, A.; Nicolini, A.M.; Monks, T.J.; Yoon, J.Y. In situ, dual-mode monitoring of organ-on-a-chip with smartphone-based fluorescence microscope. Biosens. Bioelectron. 2016, 86, 697–705.

57. Roblyer, D. Perspective on the increasing role of optical wearables and remote patient monitoring in the COVID-19 era and beyond. J. Biomed. Opt. 2020, 25, 102703.
58. El Asnaoui, K.; Chawki, Y. Using X-ray images and deep learning for automated detection of coronavirus disease. J. Biomol. Struct. Dyn. 2021, 39, 3615–3626.
59. Hemdan, E.E.D.; Shouman, M.A.; Karar, M.E. Covidx-net: A framework of deep learning classifiers to diagnose COVID-19 in X-ray images. arXiv 2020, arXiv:2003.11055.
60. Shi, F.; Wang, J.; Shi, J.; Wu, Z.; Wang, Q.; Tang, Z.; He, K.; Shi, Y.; Shen, D. Review of artificial intelligence techniques in imaging data acquisition, segmentation, and diagnosis for COVID-19. IEEE Rev. Biomed. Eng. 2020, 14, 4–15.
61. Xu, X.; Jiang, X.; Ma, C.; Du, P.; Li, X.; Lv, S.; Yu, L.; Ni, Q.; Chen, Y.; Su, J.; et al. A deep learning system to screen novel coronavirus disease 2019 pneumonia. Engineering 2020, 6, 1122–1129.
62. Jamshidi, M.; Lalbakhsh, A.; Talla, J.; Peroutka, Z.; Hadjilooei, F.; Lalbakhsh, P.; Jamshidi, M.; La Spada, L.; Mirmozafari, M.; Dehghani, M.; et al. Artificial intelligence and COVID-19: Deep learning approaches for diagnosis and treatment. IEEE Access 2020, 8, 109581–109595.
63. O'Connor, T.; Javidi, B. COVID-19 screening with digital holographic microscopy using intra-patient probability functions of spatio-temporal bio-optical attributes. Biomed. Opt. Express 2022, 13, 5377–5389.
64. Shamout, F.E.; Shen, Y.; Wu, N.; Kaku, A.; Park, J.; Makino, T.; Jastrzębski, S.; Witowski, J.; Wang, D.; Zhang, B.; et al. An artificial intelligence system for predicting the deterioration of COVID-19 patients in the emergency department. NPJ Digit. Med. 2021, 4, 80.
65. Barnawi, A.; Chhikara, P.; Tekchandani, R.; Kumar, N.; Alzahrani, B. Artificial intelligence-enabled Internet of Things-based system for COVID-19 screening using aerial thermal imaging. Future Gener. Comput. Syst. 2021, 124, 119–132.
66. Carvalho, L.F.d.C.e.S.; Nogueira, M.S. Optical techniques for fast screening-Towards prevention of the coronavirus COVID-19 outbreak. Photodiagnosis Photodyn. Ther. 2020, 30, 101765.
67. Rai, M.; Deshmukh, S.D.; Ingle, A.P.; Gupta, I.R.; Galdiero, M.; Galdiero, S. Metal nanoparticles: The protective nanoshield against virus infection. Crit. Rev. Microbiol. 2016, 42, 46–56.
68. Łoczechin, A.; Séron, K.; Barras, A.; Giovanelli, E.; Belouzard, S.; Chen, Y.T.; Metzler-Nolte, N.; Boukherroub, R.; Dubuisson, J.; Szunerits, S. Functional carbon quantum dots as medical countermeasures to human coronavirus. ACS Appl. Mater. Interfaces 2019, 11, 42964–42974.
69. Wainwright, M. Local treatment of viral disease using photodynamic therapy. Int. J. Antimicrob. Agents 2003, 21, 510–520.
70. Kharkwal, G.B.; Sharma, S.K.; Huang, Y.Y.; Dai, T.; Hamblin, M.R. Photodynamic therapy for infections: Clinical applications. Lasers Surg. Med. 2011, 43, 755–767.

71. Agostinis, P.; Berg, K.; Cengel, K.A.; Foster, T.H.; Girotti, A.W.; Gollnick, S.O.; Hahn, S.M.; Hamblin, M.R.; Juzeniene, A.; Kessel, D.; et al. Photodynamic therapy of cancer: An update. CA Cancer J. Clin. 2011, 61, 250–281.
72. Fekrazad, R. Photobiomodulation and antiviral photodynamic therapy as a possible novel approach in COVID-19 management. Photobiomodulation Photomed. Laser Surg. 2020, 38, 255–257.